Decoupling of spurious deeply bound states with the similarity renormalization group

K. A. Wendt, R. J. Furnstahl, and R. J. Perry

Decoupling of Spurious Deeply Bound States with the Similarity Renormalization Group

K.A. Wendt,[*] R.J. Furnstahl,[†] and R.J. Perry[‡]

Department of Physics, The Ohio State University, Columbus, OH 43210

(Dated: February 15, 2011)

The Similarity Renormalization Group (SRG) is a continuous series of unitary transformations that can be implemented as a flow equation. When the relative kinetic energy ($T_{\rm rel}$) is used in the SRG generator, nuclear structure calculations have shown greatly improved convergence with basis size because of the decoupling of high-energy and low-energy physics. However this generator can sometimes be problematic. A test case is provided by a study of initial interactions from chiral effective field theories with large cutoffs, which can lead to spurious deeply bound states. We would like the SRG to decouple these from the physical shallow bound states. However, with $T_{\rm rel}$ the high- and low-energy bound states are not decoupled in the usual sense. Replacing $T_{\rm rel}$ by the momentum-space diagonal of the Hamiltonian (H_d) in the SRG generator does produce decoupling, such that the shallow states are in the low-momentum region and the deeply bound states are at higher momentum. The flow toward universal low-momentum interactions is also restored.

I. INTRODUCTION

Similarity Renormalization Group (SRG) flow equations with a generator based on the relative kinetic energy have been shown to soften inter-nucleon interactions by decoupling energy scales [1, 2], leading to significantly enhanced convergence in calculations of nuclear structure and reactions [2–8]. To date, these SRG applications have all started with phenomenological potentials such as Argonne v_{18} [9] or the next-to-next-to-next-to-leading order (N³LO) chiral potentials from Refs. [10] and [11]. When evolved to softened form, matrix elements of these interactions are found to collapse toward a common NN potential for momenta below the decoupling scale [2]. These desirable SRG features are not guaranteed, however, when applied to chiral effective field theory (EFT) interactions with large cutoffs. Such interactions have been explored at leading order [12] to examine renormalization issues (see also Refs. [13–19]). The SRG approach as applied so far to nuclear interactions fails for these theories in channels where the tensor force from pion exchange introduces spurious deeply bound states. The generic cause of this failure was identified by Glazek and Perry [20]. In this paper we document the specific problems with large-cutoff chiral EFT ($\chi_{\rm EFT}$) and test whether they are fixed as described in Ref. [20].

The SRG as used here is implemented as a series of infinitesimal unitary transforms of a Hamiltonian H, labeled by a flow parameter s [21, 22],

$$H(s) = U(s)H(s = 0)U^\dagger(s) . \tag{1}$$

Differentiating with respect to the flow parameter shows how any evolution is constrained by unitarity,

$$\frac{d}{ds}H(s) = [\eta(s), H(s)] , \tag{2}$$

where

$$\eta(s) = \frac{dU(s)}{ds}U^\dagger(s) . \tag{3}$$

The flow is controlled through the choice of the anti-Hermitian generator $\eta(s)$. To generate a renormalization group evolution, we need the flow to decouple high and low energy degrees of freedom (i.e. to remove far off diagonal matrix elements). For many applications, a useful form for the generator is

$$\eta(s) = [G(s), H(s)] , \tag{4}$$

where $G(s)$ is a Hermitian operator. The original choice for $G(s)$ advocated by Wegner and collaborators [21, 22] and applied extensively in condensed matter is the diagonal component of the interaction, $G(s) = H_d(s)$,

$$\langle i|H_d(s)|j\rangle \equiv \begin{cases} \langle i|H(s)|i\rangle & \text{if } i = j , \\ 0 & \text{otherwise.} \end{cases} \tag{5}$$

If the basis in which H_d is taken to be diagonal is a discretized, partial-wave momentum basis $|i\rangle \equiv |k_i lm\rangle$, the Hamiltonian is driven toward diagonal form with s such that the parameter $\lambda \equiv s^{-1/4}$ is a measure of the width of diagonal [21, 22].

In most applications to nuclear systems, $G(s)$ has been taken simply to be the relative kinetic energy $T_{\rm rel}$, which is by construction independent of s. This choice also has the effect in practice of driving the momentum-space potential toward the diagonal, which directly softens the repulsive core of nucleon-nucleon interactions (as well as short-range tensor forces) by decoupling high- and low-momentum degrees of freedom [1]. No adverse results have been observed for light nuclei; however, this SRG evolution has always been terminated such that $\lambda \geq 1$ fm^{-1}.

In Ref. [20], it was observed that when evolving a simple model Hamiltonian, the Wegner evolution ($G = H_d$) will decouple the bound state by leaving it as an isolated

eigenvalue on the diagonal of the Hamiltonian matrix. In contrast, they found a very different behavior with the evolution generated using $T_{\rm rel}$. With $T_{\rm rel}$, the bound state remains coupled to low momentum, and is pushed to the lowest momentum part of the matrix. This undesirable result has not been seen in the two-nucleon system for $\lambda \geq 1$ fm^{-1} because the only physical bound state, the deuteron, is very shallow (e.g., the scattering length in this channel is unnaturally large) and only plays a role for $\lambda \ll 1$ fm^{-1}. Indeed, the evolution for $T_{\rm rel}$ and H_d in the usual range of λ is practically identical numerically (at least for the $A = 2$ system).

In most cases, we do not want to decrease λ to the point where bound-state eigenvalues appear on the diagonal. The effects of discretized momenta are magnified when H is driven too close to diagonal form, so we typically seek a window in which high-energy states decouple but the low-energy part of H is insensitive to discretization. However, if a spurious deeply bound state exists because our effective Hamiltonian is singular at short distances, we want to make sure that any associated spurious physics decouples from the low-energy physics our effective theory is intended to capture. In this way the practical advantages of the SRG are preserved. This is accomplished if the spurious bound eigenstate is forced to the diagonal when λ is still sufficiently above the scale of interest. According to Glazek and Perry, this happens for the H_d-based generator but $T_{\rm rel}$ drives the bound-state eigenvalue to the low-energy corner of the Hamiltonian matrix [20]. As a result, H_d decouples the spurious state from low-energy physics but $T_{\rm rel}$ causes the spurious state to corrupt low-energy physics.

In this paper, we test whether the analysis of Glazek and Perry carries over to the nuclear case with spurious bound states and further investigate the nature of decoupling and the flow toward universal interactions in the SRG. In Section II, we give background details on the leading-order chiral EFT that is the laboratory for our analysis. In Section III, we examine decoupling for the deuteron and phase shifts starting from the LO EFT. The implications are discussed in Section IV and we summarize in Section V.

II. BACKGROUND

A. Chiral EFT at Leading Order

An implementation of chiral EFT at leading order (LO) in Weinberg's power counting was studied in Ref. [12] for a large range of momentum cutoffs $\Lambda_{\rm EFT}$ to determine what renormalization was needed in each partial wave to achieve cutoff independence. The EFT NN potential at LO consists of one-pion exchange in all channels plus a regulated contact interaction in certain channels; it is meant to be iterated to all orders. The power counting proposed by Weinberg included contact interactions in only the S-waves at LO, but this was found

by Nogga et al. to be inadequate for cutoff independence in partial waves that have an attractive tensor force (for high enough angular momentum there is no problem). Adding a single contact interaction in applicable channels remedied this problem and allowed large cutoffs to be explored.

A side effect of the attractive tensor force was the appearance with increasing $\Lambda_{\rm EFT}$ of spurious deeply bound states. These are not a problem in principle for the EFT, because they appear outside its domain of validity. That is, the EFT is expected to have incorrect ultraviolet (UV) behavior, whose impact on low-energy observables is corrected by the contact counterterms. In this case, UV refers to large negative as well as positive high energies. In practice the problems caused by spurious deeply bound states for solving few-body equations led Nogga et al. to remove them by hand [12]. Our question here is: Can these deeply bound states be decoupled by renormalization group flow equations? This question makes the LO chiral EFT Hamiltonian a good test case to study the robustness of the observations in Ref. [20] and to learn about the decoupling properties of the SRG as a function of $\Lambda_{\rm EFT}$. The present study is restricted to two-particle systems. The impact on three- and higher-particle systems may be of even greater interest, but is deferred to future work.
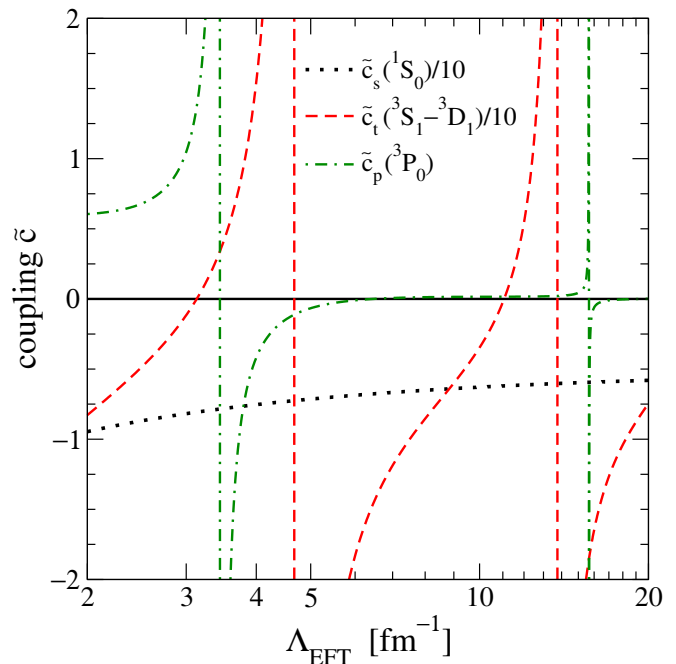

FIG. 1. (color online) Dimensionless coupling constants for the LO chiral EFT as a function of the EFT cutoff $\Lambda_{\rm EFT}$. For the $^1S_0$ channel, $\tilde{c}_s \equiv c_s/f_\pi^2$ is fit to the phase shift at $E_{\rm lab} = 10$ MeV. For the coupled $^3S_1$–$^3D_1$ channel, $\tilde{c}_t \equiv c_t/f_\pi^2$ is fit to the $^3S_1$ phase shift at 10 MeV. The constant $\tilde{c}_p \equiv c_p/f_\pi^4$ is fit to the $^3P_0$ phase shift at 50 MeV.

We follow Ref. [12] in defining the LO chiral EFT. For

all our calculations, we regulated the interaction with

$$f_n(k, k') = e^{-(k/\Lambda_{\rm EFT})^{2n}} e^{-(k'/\Lambda_{\rm EFT})^{2n}} , \qquad (6)$$

using $n = 4$. Our notation differs from Ref. [12] only in the definition of dimensionless coupling constants (see Fig. 1 caption). We focus on three channels, which are sufficient for the present discussion. The $^1S_0$ channel is an example of a partial wave where the tensor force does not contribute and therefore has no spurious bound states. The coupled $^3S_1-^3D_1$ channel and the $^3P_0$ channel provide representative examples of partial waves with an attractive tensor force; each develops spurious bound states with increasing $\Lambda_{\rm EFT}$ in addition to the physical deuteron in the coupled channel.
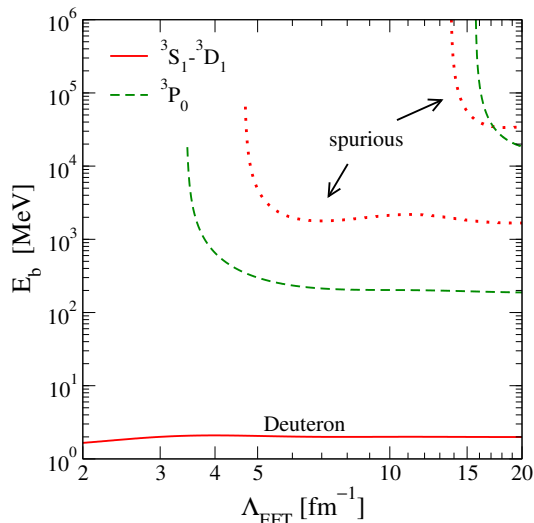

FIG. 2. (color online) Bound-state energies as a function of $\Lambda_{\rm EFT}$ for the $^3S_1-^3D_1$ coupled channel (deuteron as a solid line, spurious states as dotted lines) and the $^3P_0$ channel (spurious states as dashed lines).

For the singlet and triplet S-waves we fit the coupling constants to the neutron-proton phase shifts at $E_{\rm lab} = 10$ MeV, and for the $^3P_0$ channel we fit to the $E_{\rm lab} = 50$ MeV phase shift. The couplings in these channels are shown in Fig. 1 and the bound state energies in Fig. 2, each as functions of $\Lambda_{\rm EFT}$. We see that the running of the coupling constant in the $^1S_0$ channel is quite mild throughout the range of $\Lambda_{\rm EFT}$. In contrast, the running in each of the other channels displays a limit-cycle pattern. With each cycle to $+\infty$ a new bound state emerges, at energies bound by two hundred MeV or much more, which place them outside the low-energy domain of the EFT.

In Figs. 3, 4, and 5 we plot the phase shifts for representative values of $\Lambda_{\rm EFT}$ up to a lab energy of 100 MeV. Because the EFT is only evaluated at leading order, we should not be surprised at large deviations compared to experiment (here represented by the Nijmegen partial wave analysis). However, our interest is not in establishing how well experiment is reproduced, but in how
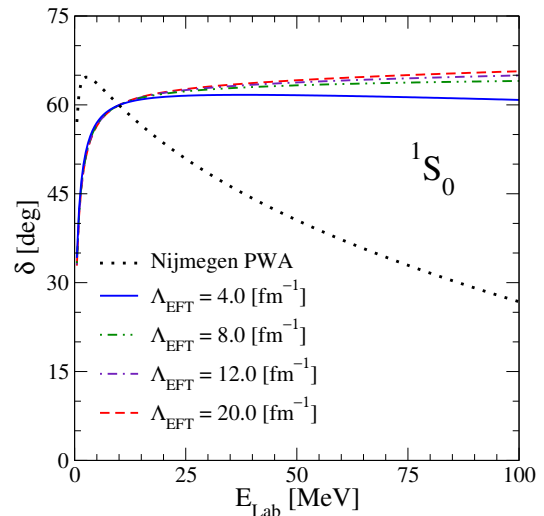

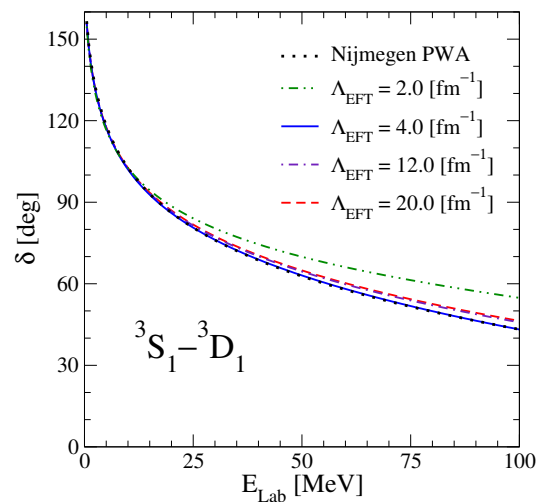FIG. 3. (color online) $^1S_0$ phase-shifts as a function of laboratory energy for several different $\Lambda_{\rm EFT}$.

FIG. 4. (color online) $^3S_1$ phase-shifts as a function of laboratory energy for several different $\Lambda_{\rm EFT}$.

close the predictions of the various Hamiltonians are to each other as a function of interaction energy. This will be relevant when we examine universality below.

III. RESULTS

In this section, we evolve LO chiral EFT potentials at representative cutoffs using flow equations with generators based on both $T_{\rm rel}$ and H_d. We start with the $^1S_0$ channel, for which there are no spurious bound states. As illustrated in Fig. 6 for a cutoff of $\Lambda_{\rm EFT} = 8.0$ fm^{-1}, the evolved potentials for $T_{\rm rel}$ and H_d are practically indistinguishable. This is true at any cutoff for this channel. More generally we have found it to be true for any channel for which there are no spurious bound states.

A very different story as a function of $\Lambda_{\rm EFT}$ is found in the coupled $^3S_1-^3D_1$ channel, as seen in Figs. 7, 8,
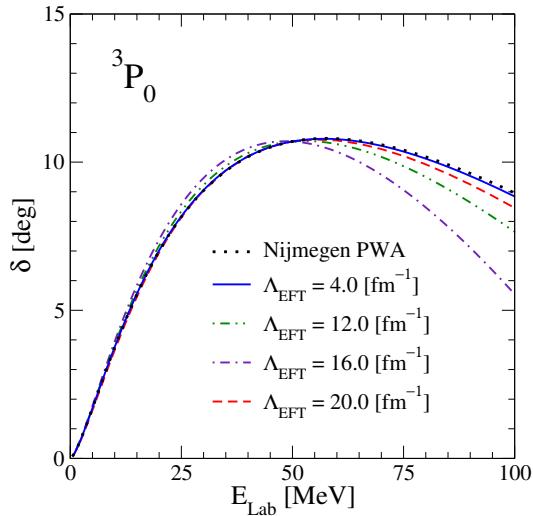
FIG. 5. (color online) $^3P_0$ phase-shifts as a function of laboratory energy for several different $\Lambda_{\rm EFT}$.

and 9, which compare the $T_{\rm rel}$ and H_d evolutions for $\Lambda_{\rm EFT} = 4.0$, 9.0, and 20.0 fm^{-1}, respectively. The initial $\Lambda_{\rm EFT} = 4.0$ fm^{-1} interaction supports only the deuteron bound state. Without any spurious states to decouple, the evolutions generated by $T_{\rm rel}$ and H_d are nearly identical to each other, as with $^1S_0$. However, in Fig. 8 there is now a spurious state to decouple and so the SRG evolution for $T_{\rm rel}$ and H_d are substantially different.

Both the $T_{\rm rel}$ and H_d evolutions steadily drive the matrix toward a diagonal form. In the process, the low momentum part of the matrix is driven towards large negative values. With $T_{\rm rel}$ this is unabated, while in the H_d evolution it reverses momentarily and deposits an isolated negative eigenvalue on the diagonal, which corresponds to the complete decoupling of this spurious state [20]. The low-momentum potential in the last two panels of Fig. 8 for $T_{\rm rel}$ (bottom) is qualitatively different from the corresponding panels for $\Lambda_{\rm EFT} = 4.0$ fm^{-1} in Fig. 7 while the corresponding H_d panels are similar for momenta below the spurious state matrix element.

Figure. 9 shows what happens when a second spurious state is supported after increasing the EFT cutoff to $\Lambda_{\rm EFT} = 20.0$ fm^{-1}. Again $T_{\rm rel}$ and H_d differ significantly but the latter is similar to H_d in the other figures. If we expanded the momentum scales, we would find that the deepest state is first decoupled, with the diagonal element found at much larger k, and then the shallower spurious state is decoupled at smaller λ.

For the uncoupled $^3P_0$ channel, the tensor is also attractive and increasing the cutoff of the EFT leads to a spurious bound state for $\Lambda_{\rm EFT}$ between 3 and 4 fm^{-1}. In Figs. 10, 11, and 12 we trace the evolution for two cutoffs above the threshold for a single bound state ($\Lambda_{\rm EFT} = 4$ fm^{-1} and $\Lambda_{\rm EFT} = 8$ fm^{-1}), and for a third above the threshold for two bound states ($\Lambda_{\rm EFT} = 20$ fm^{-1}). Results for low cutoffs with no bound states are not shown, but have the same pattern as for $^1S_0$. With a spuri-

ous state to decouple, the SRG evolutions for $T_{\rm rel}$ and H_d at the lowest $\Lambda_{\rm EFT}$ are again substantially different, just as for the $^3S_1$–$^3D_1$ channel. We see particularly non-universal evolution of the low-momentum part of the $T_{\rm rel}$ potentials while the H_d potentials are similar (more quantitative comparisons are made below). Note that the diagonalization of the spurious bound states do not occur at the same diagonal momentum.

The quantitative evolution can be characterized by focusing on the diagonal and fully off-diagonal matrix elements separately. In Figs. 13 and 14 the diagonal and fully off-diagonal matrix elements of the interactions in the $^3S_1$ are plotted for H_d and $T_{\rm rel}$, respectively, as representative examples. The decoupling of high and low momentum degrees of freedom is a prevalent feature in the Wegner evolution whether there is a deeply bound state or not. The result of this decoupling is that the low momentum portion of the matrix becomes universal, with a collapse of the original potentials to almost the same low-k dependence for sufficiently low λ. In contrast, with the $T_{\rm rel}$ evolution the low-momentum diagonal matrix elements are always quite distinct. The plots showing the off-diagonal edge manifest the distinction most clearly because the non-universal off-diagonal elements above λ are driven to zero. Similar behavior is observed in other channels. The degree of collapse with the Wegner evolution is correlated with the level of agreement of the phase shifts in that channel.

Figure 15 shows similarly striking consequences of the choice of generator for the momentum distributions of the bound states in the $^3S_1$–$^3D_1$ channel, with $\Lambda_{\rm EFT} = 20$ fm^{-1} and an evolution to $\lambda = 1.2$ fm^{-1} chosen as a representative case. The initial deuteron momentum distribution has a nearly exponential tail while the spurious state is essentially flat in the region of momenta plotted (reflecting the confinement of the coordinate-space wavefunction). Their fates after evolution with $T_{\rm rel}$ and H_d are starkly different. In the former case (left panel), the spurious state has had its strength pushed to low momentum while the deuteron becomes broadly distributed and qualitatively changed at low momentum. In the latter case (right panel), the spurious state is confined to a small region in momentum near $k = 1.6$ fm^{-1} while the deuteron momentum distribution at low momentum is essentially unchanged. Similar results are found with other choices of $\Lambda_{\rm EFT}$.

The phase shifts for a given $\Lambda_{\rm EFT}$ are unchanged as a result of a unitary SRG evolution. However, we can test the degree of decoupling in different cases by cutting the evolved potential (i.e., setting it to zero for all k, k' above a cut momentum) and looking at the degradation in the phase shifts. This is shown in Figs. 16, 17, 18 for the $^3S_1$ phases shifts evolved from $\Lambda_{\rm EFT} = 4$, 9, and 20 fm^{-1}, respectively. The cut is implemented by multiplying each matrix element by the factor $e^{-(k/\Lambda)^{2m}}e^{-(k'/\Lambda)^{2m}}$. Results for $m = 2, 4, 8$ are similar; we show $m = 4$ only. In general, successful decoupling means that the phase shifts calculated with a potential evolved to λ are unchanged
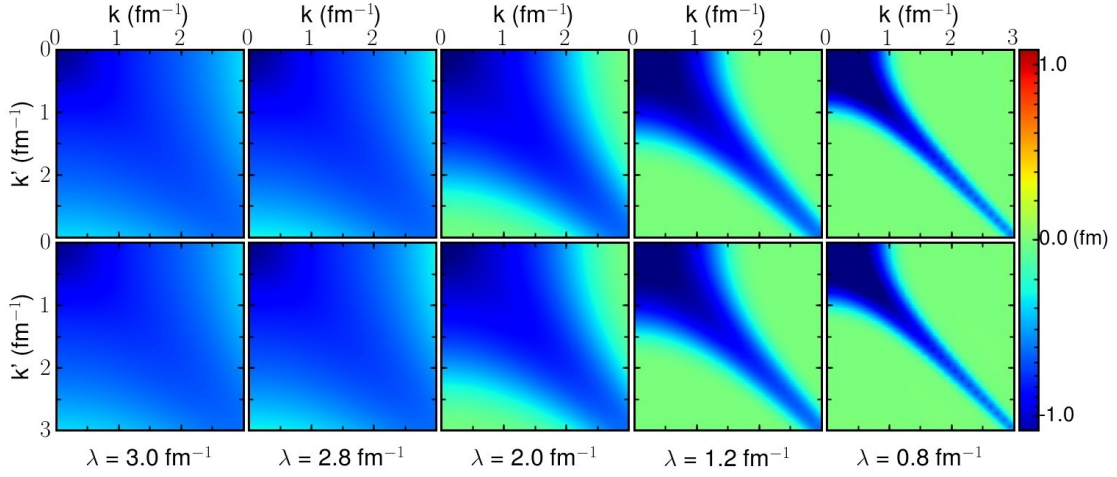
FIG. 6. (color online) Contour plot of $V_\lambda(k, k')$ in the $^1S_0$ channel for $\chi_{\rm EFT}$ with a cutoff of $\Lambda_{\rm EFT} = 8.0\,{\rm fm}^{-1}$ for $T_{\rm rel}$ (top) and H_d (bottom) SRG evolution.
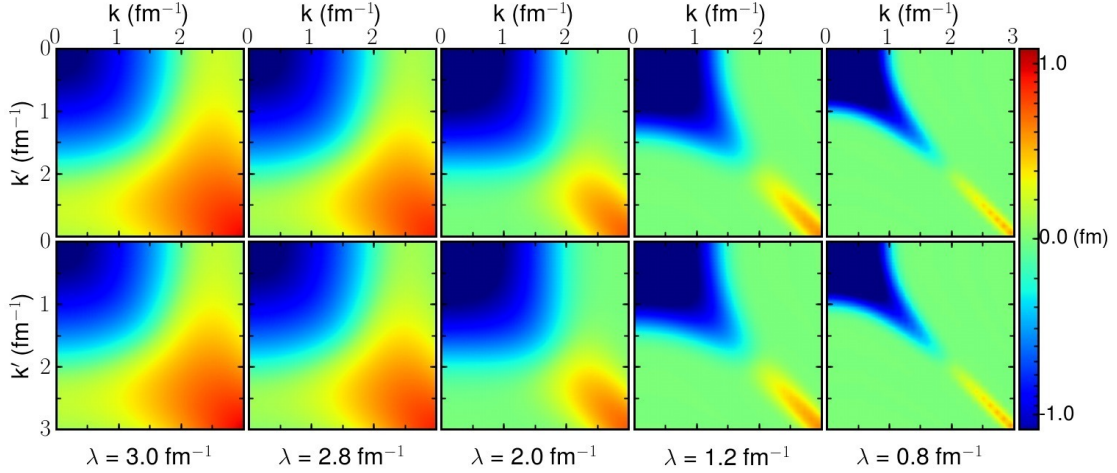
FIG. 7. (color online) Contour plot of $V_\lambda(k, k')$ in the $^3S_1$ channel for $\chi_{\rm EFT}$ with a cutoff of $\Lambda_{\rm EFT} = 4.0\,{\rm fm}^{-1}$ for $T_{\rm rel}$ (top) and H_d (bottom) SRG evolution.
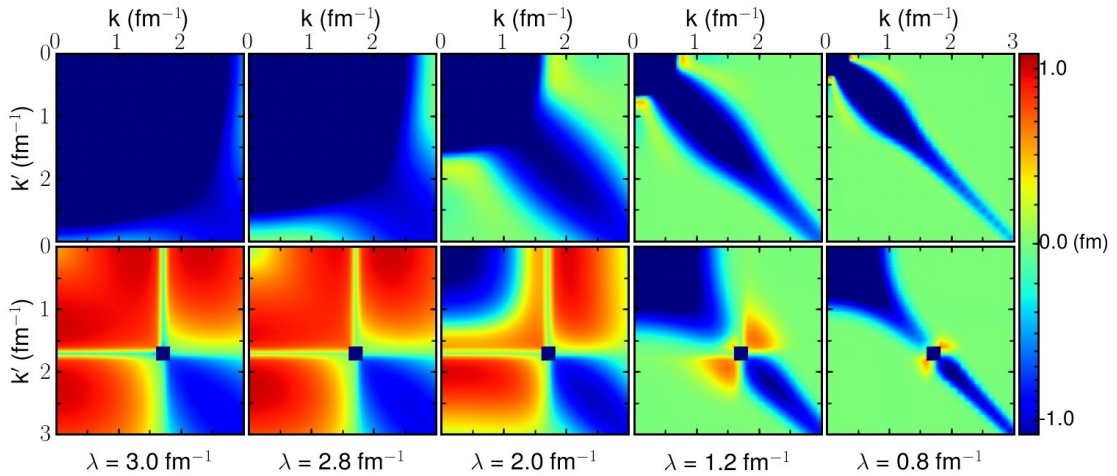
FIG. 8. (color online) Contour plot of $V_\lambda(k, k')$ in the $^3S_1$ channel for $\chi_{\rm EFT}$ with a cutoff of $\Lambda_{\rm EFT} = 9.0\,{\rm fm}^{-1}$ for $T_{\rm rel}$ (top) and H_d (bottom) SRG evolution.

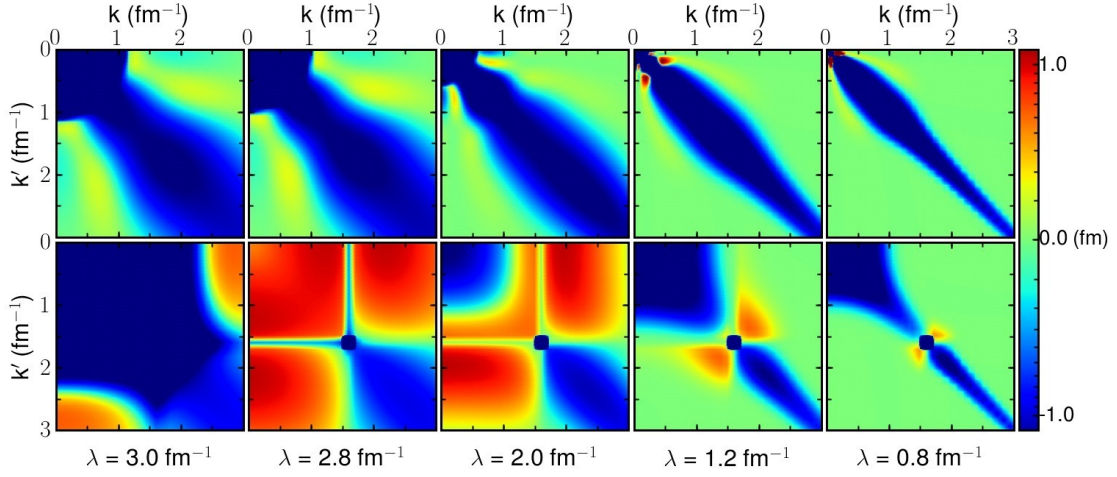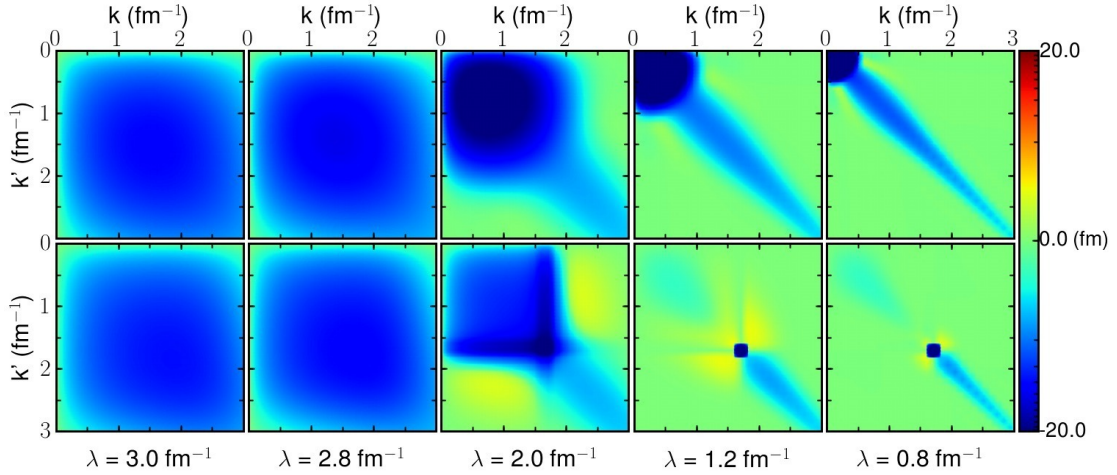at low energy if $\lambda < \Lambda$ (of course they will deviate for   energies above the cut).

FIG. 9. (color online) Contour plot of $V_\lambda(k, k')$ in the $^3S_1$ channel for χ_{EFT} with a cutoff of $\Lambda_{\text{EFT}} = 20.0\,\text{fm}^{-1}$ for T_{rel} (top) and H_d (bottom) SRG evolution.

FIG. 10. (color online) Contour plot of $V_\lambda(k, k')$ in the $^3P_0$ channel for χ_{EFT} with a cutoff of $\Lambda_{\text{EFT}} = 4.0\,\text{fm}^{-1}$ for T_{rel} (top) and H_d (bottom) SRG evolution.

If there are no spurious bound states, decoupling works for either T_{rel} or H_d evolution, as seen in Fig. 16. In particular, the phase shifts are essentially unchanged for $\lambda \le 2.0\,\text{fm}^{-1}$ after a $2.5\,\text{fm}^{-1}$ cut and agree at low energy after a $1.5\,\text{fm}^{-1}$ cut for sufficiently low λ. The pattern of decoupling is similar for H_d-evolved potentials when there are spurious bound states, except that the onset of decoupling is delayed until λ is sufficiently below where the bound state is deposited on the diagonal. Thus, in the top panels of Figs. 17 and 18, decoupling is not achieved until $\lambda = 1.2\,\text{fm}^{-1}$, compared to $\lambda = 2.0\,\text{fm}^{-1}$ in Fig. 16 for the $2.5\,\text{fm}^{-1}$ cut. This may slow convergence in few- or many-body calculations; this remains to be investigated. The decoupling patterns for phases shifts calculated from T_{rel}-evolved potentials with spurious bound states show serious distortions at the lower cut.

IV. DISCUSSION

We have documented several different outcomes from evolution with generators using H_d and T_{rel}. For T_{rel}, the different classes of low-momentum Hamiltonians depend on the number of spurious states, while for H_d there is a single universal class for the low-energy part, after sufficient evolution. There is corruption of the low-momentum probability distribution for T_{rel} and the physical low-lying bound state is still coupled and non-universal. In contrast, with H_d the spurious state completely decouples and the deuteron wave function is unchanged at low momentum. Note that despite these unhappy features for T_{rel}, the results for all observables are formally the same because we still have a unitary transformation acting on a renormalized Hamiltonian. In practice, however, numerical computation may lose all precision for observables influenced by the near-diagonalized part and our ability to truncate a basis ex-
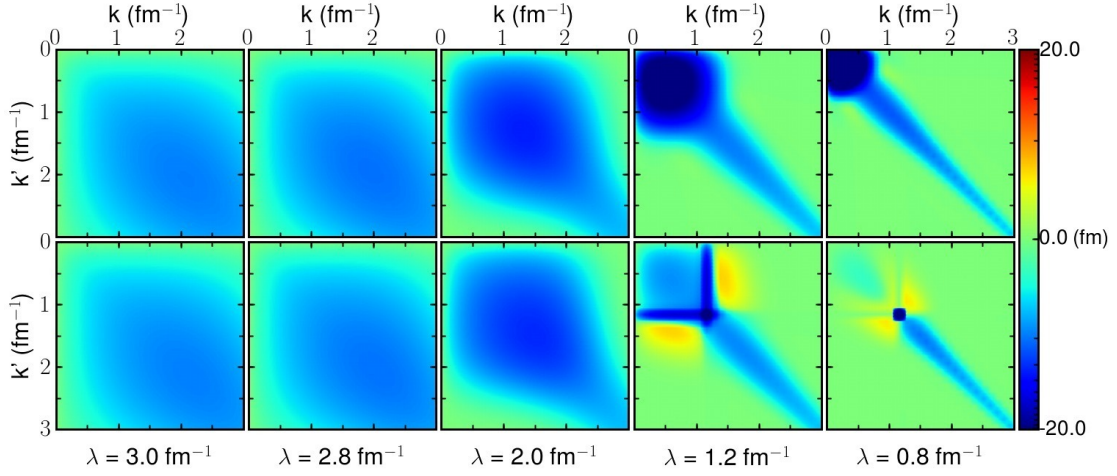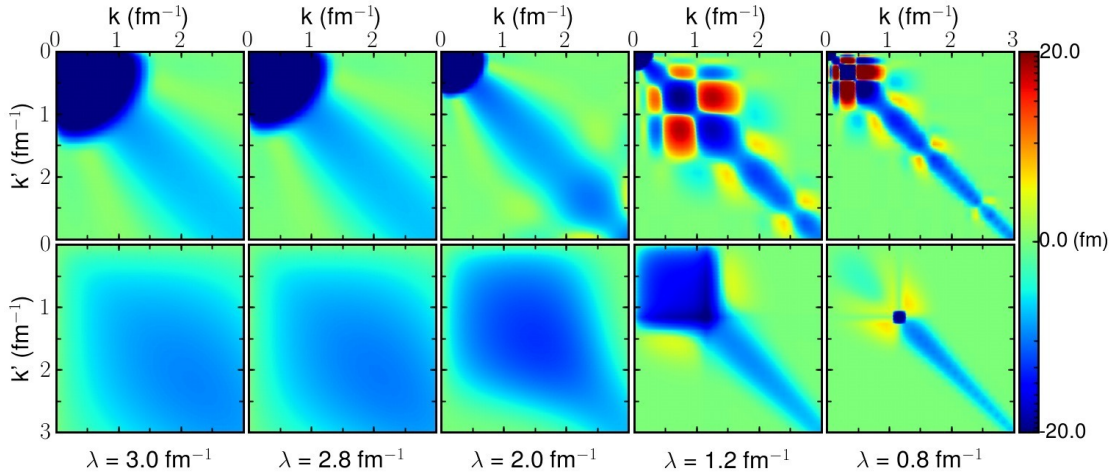
FIG. 11. (color online) Contour plot of $V_\lambda(k, k')$ in the ${}^3P_0$ channel for χ_{EFT} with a cutoff of $\Lambda_{\mathrm{EFT}} = 8.0\,\mathrm{fm}^{-1}$ for T_{rel} (top) and H_d (bottom) SRG evolution.

FIG. 12. (color online) Contour plot of $V_\lambda(k, k')$ in the ${}^3P_0$ channel for χ_{EFT} with a cutoff of $\Lambda_{\mathrm{EFT}} = 20.0\,\mathrm{fm}^{-1}$ for T_{rel} (top) and H_d (bottom) SRG evolution.
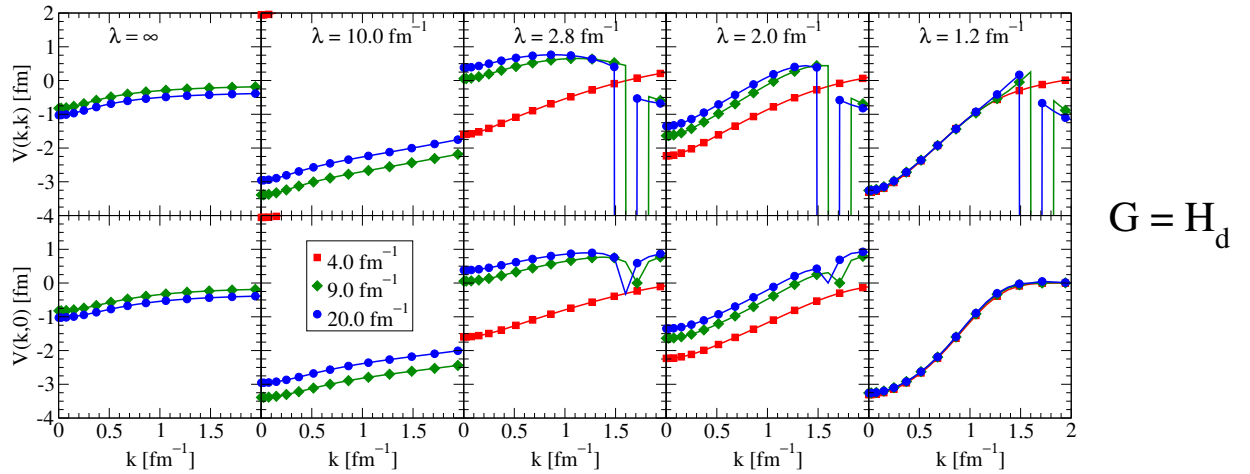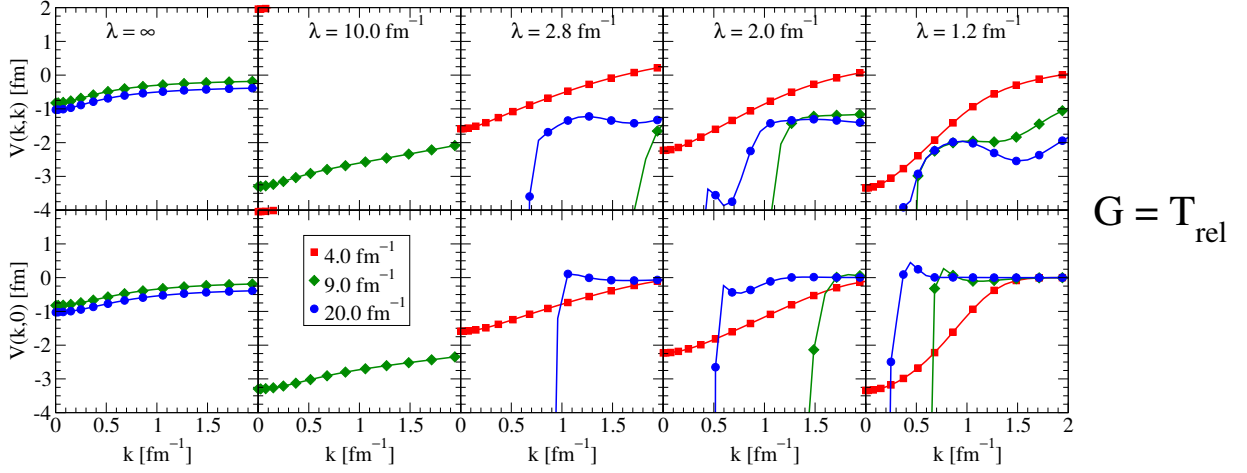

FIG. 13. (color online) The diagonal matrix elements $V_s(k, k)$ and fully off-diagonal matrix elements $V_s(k, 0)$ for the ${}^3S_1$ channel are plotted against momentum k after evolving using the Wegner generator to a range of final flow parameters $\lambda = s^{-1/4}$. For each λ, results for five cutoff values Λ_{EFT} are shown (in some cases they are beyond the limits of the plot).

FIG. 14. (color online) The diagonal matrix elements $V_s(k,k)$ and fully off-diagonal matrix elements $V_s(k,0)$ for the $^3S_1$ channel are plotted against momentum k after evolving using the T_{rel}–based generator to a range of final flow parameters $\lambda = s^{-1/4}$. For each λ, results for five cutoff values Λ_{EFT} are shown (in some cases they are beyond the limits of the plot).
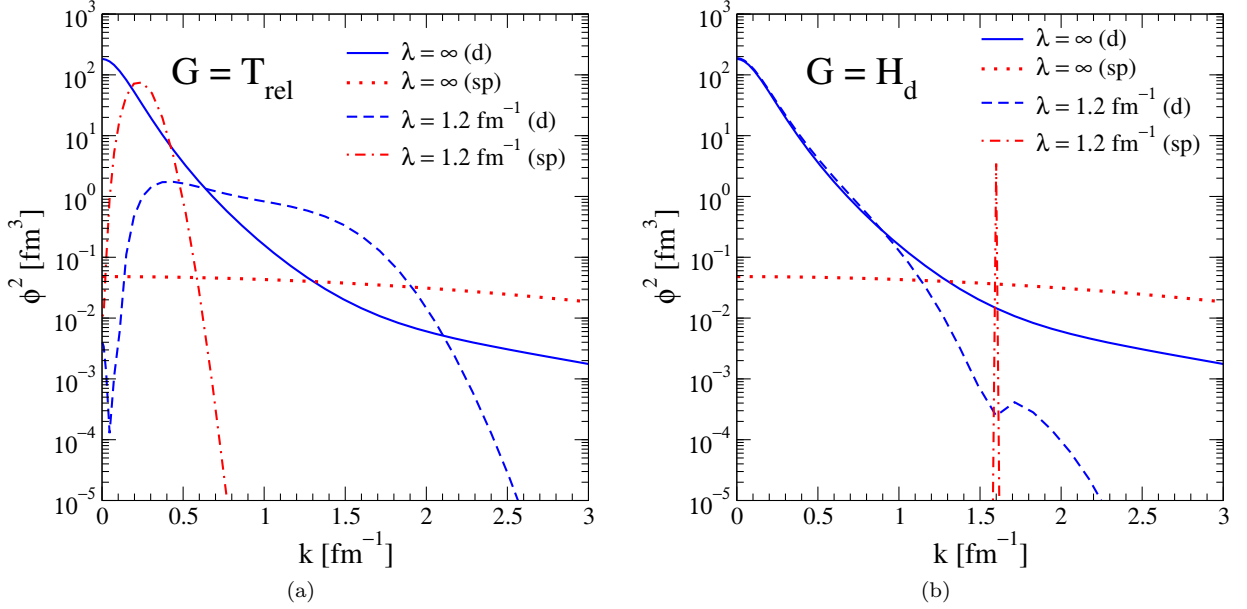

FIG. 15. (color online) Momentum probability densities in the coupled $^3S_1$–$^3D_1$ channel with $\Lambda_{EFT} = 20$ fm^{-1} for the deuteron (d) and shallowest spurious state (sp). On the left are the initial and evolved densities using the T_{rel} generator evolved to $\lambda = 1.2$ fm^{-1} while on the right are the same densities but evolved using the H_d generator.

pansion will be compromised.

Although it is clear that decoupling increases with decreasing λ when using H_d, it may not be so useful in practice. The binding energies of the spurious states seen here are very large, yet the decoupling momenta for the least bound ones are still comparable or smaller than values where SRG evolution is usually halted because of concerns about the growth of many-body forces. Will the remaining distortions spoil the advantages? For example, are variational calculations still effective and is convergence in basis expansions still accelerated? Answering these questions will require extending our tests to $A \geq 3$. Also, the question of where a bound state is

placed on the diagonal in momentum representation is still open.

In Sect. II we invoked the claim that the deeply bound states are outside the range of the EFT and as a result should not disturb the low-energy EFT predictions. Our results provide an explicit test of this principle. In particular, the SRG unitary flow does not change the S-matrix and yet with an H_d-based generator we are able to create a decoupled version of the Hamiltonian. Because it becomes decoupled at a finite momentum scale λ and has the same universal form in the low-energy region as potentials with no spurious bound states, we have achieved the desired demonstration.
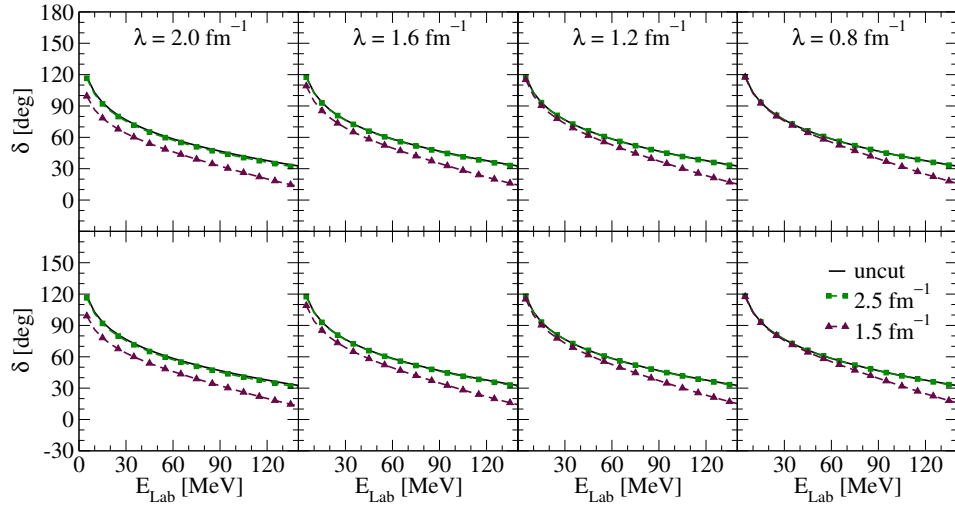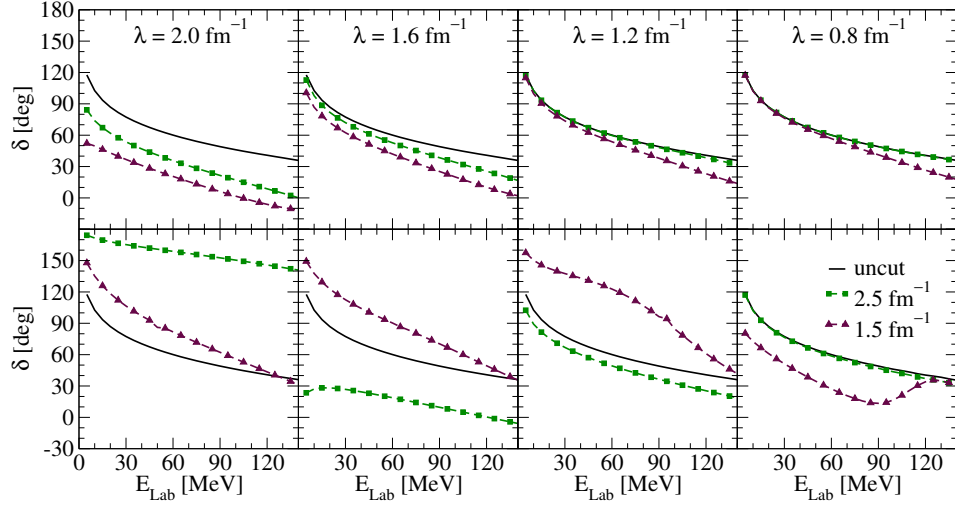
FIG. 16. (color online) Phase shifts in the coupled $^3S_1-^3D_1$ channel using the $\Lambda_{\mathrm{EFT}} = 4.0$ fm^{-1} potential, testing H_d (top) and T_{rel} (bottom) SRG decoupling by first cutting off the potential.

FIG. 17. (color online) Phase shifts in the coupled $^3S_1-^3D_1$ channel using the $\Lambda_{\mathrm{EFT}} = 9.0$ fm^{-1} potential, testing H_d (top) and T_{rel} (bottom) SRG decoupling by first cutting off the potential.
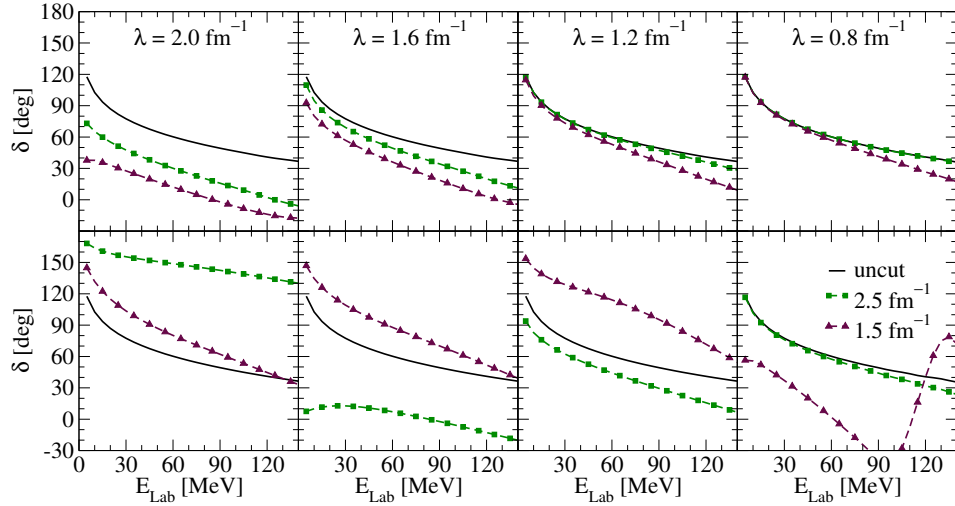

FIG. 18. (color online) Phase shifts in the coupled $^3S_1-^3D_1$ channel using the $\Lambda_{\mathrm{EFT}} = 20.0$ fm^{-1} potential, testing H_d (top) and T_{rel} (bottom) SRG decoupling by first cutting off the potential.

An important open question is the impact on SRG evolution of bound states for $A > 2$. For example, at what λ do we expect to have problems evolving with a T_{rel}-based generator for the triton, ^{4}He, or nuclear matter? The choice between T_{rel} and H_d for building the SRG generator is just one of many possible useful choices to control the flow of the Hamiltonian. What other generators achieve what H_d does but allow more freedom? Work is in progress to address these issues.

V.   SUMMARY

In this paper, we have applied SRG evolution flow equations that have been uniformly successful with commonly used initial NN interactions to a new class of initial potentials. These potentials are from renormalized leading-order chiral EFT and have much higher momentum-space cutoffs which, combined with singular pion exchange, lead to spurious bound states emerging in channels where there is a non-zero, attractive tensor force. We have tested flow properties such as decoupling and the approach to universal form.

While the choice of T_{rel} in the SRG generator has been successful for nuclear applications to date, this has been the fortuitous result of shallow bound states that are not disturbed for the λ's considered. The presence of deeply bound states introduces problems first emphasized by Glazek and Perry [20]. The generalization to H_d restores the good features such as decoupling and flow to a universal form as λ decreases.

An important moral is that even a comparatively subtle change in the generator can have a substantial effect on the flow of the Hamiltonian. While in principle observables are always unchanged because we are making unitary transformations, in practice there are always truncations that make the transformations only approximately unitary. It is critical to minimize the impact of these approximations as we extend calculations to more particles. At the same time, the degree of perturbativeness and convergence properties of the Hamiltonian can also be significantly affected. Future work includes looking at few-body systems and using the SRG in further investigations of EFT.

ACKNOWLEDGMENTS

[1] E. D. Jurgenson, S. K. Bogner, R. J. Furnstahl, and R. J. Perry, Phys. Rev. C **78**, 014003 (2008).

[2] S. K. Bogner, R. J. Furnstahl, and A. Schwenk, Prog. Part. Nucl. Phys. **65**, 94 (2010).

[3] S. K. Bogner *et al.*, Nucl. Phys. A **801**, 21 (2008).

[4] E. D. Jurgenson, P. Navratil, and R. J. Furnstahl, Phys. Rev. Lett. **103**, 082501 (2009).

[5] E. D. Jurgenson, P. Navratil, and R. J. Furnstahl, (2010), arXiv:1011.4085 [nucl-th].

[6] K. Hebeler, S. K. Bogner, R. J. Furnstahl, A. Nogga, and A. Schwenk, (2010).

[7] P. Navratil, R. Roth, and S. Quaglioni, Phys. Rev. **C82**, 034609 (2010).

[8] P. Navratil, S. Quaglioni, and R. Roth, (2010).

[9] R. B. Wiringa, V. G. J. Stoks, and R. Schiavilla, Phys. Rev. C **51**, 38 (1995).

[10] D. R. Entem and R. Machleidt, Phys. Rev. C **68**, 041001 (2003).

[11] E. Epelbaum, W. Glockle, and U.-G. Meissner, Nucl. Phys. A **747**, 362 (2005).

[12] A. Nogga, R. G. E. Timmermans, and U. van Kolck, Phys. Rev. C **72**, 054006 (2005).

[13] M. Pavon Valderrama and E. R. Arriola, Phys. Rev. **C74**, 054001 (2006).

[14] M. Pavon Valderrama and E. Ruiz Arriola, Phys. Rev. **C72**, 054002 (2005).

[15] M. Pavon Valderrama and E. Ruiz Arriola, Phys. Rev. **C74**, 064004 (2006).

[16] M. Pavon Valderrama, arXiv:0912.0699 [nucl-th].

[17] C. J. Yang, C. Elster, and D. R. Phillips, PoS **CD09**, 064 (2009).

[18] R. Machleidt, P. Liu, D. R. Entem, and E. R. Arriola, Phys. Rev. **C81**, 024001 (2010).

[19] D. R. Phillips, (2010), arXiv:1010.0622 [nucl-th].

[20] S. D. Glazek and R. J. Perry, Phys. Rev. D **78**, 045011 (2008).

[21] F. Wegner, Ann. Phys. (Leipzig) **3**, 77 (1994).

[22] S. Kehrein, *The Flow Equation Approach to Many-Particle Systems* (Springer, Berlin, 2006).